Nanocomposites Derived from Phenol-Functionalized Si Nanoparticles for High Performance Lithium Ion Battery Anodes

Jeong-Kyu Lee, Mayfair C. Kung, Lynn Trahey, Michael N. Missaghi, and Harold H. Kung*

Department of Chemical and Biological Engineering, Northwestern University, 2145 Sheridan Road, Evanston, Illinois, 60208-3120

Received August 17, 2008
Revised Manuscript Received November 25, 2008

Rechargeable batteries with high storage capacity and power density have many potential applications in portable electronics, transportation, and load-leveling and storage for intermittent renewable power sources such as solar and wind power.[1−3] Li ion batteries are the most promising to capitalize on these opportunities, but much higher energy and power densities and cycling stability are still needed than what can be offered by the current graphite anodes and $LiCoO_2$ cathodes. Thus, there has been intense effort to search for alternate electrode materials, including $LiMn_{1-x}Ni_xO_2$, Li−Mn−O spinel, or olivine $LiFePO_4$ for cathodes,[4] and Li_x−M alloys (M = Sn, Si, etc.)[5−7] for anodes.

Silicon, which is cheap and has the highest gravimetric and volumetric storage capacities known ($Li_{15}Si_4 \approx 3579$ mA h/g, 8340 mA h/mL), is a very attractive candidate anode material.[8] Unfortunately, the intrinsic, ∼300% volume expansion/contraction during lithiation/delithiation causes micrometer-size Si particles to fracture, diminishing electrical contact of the particles with other electrode components and resulting in poor cycling performance.[9−11] The volume expansion/contraction is better accommodated with nanosize structures, such as nanoparticles,[12] thin films,[13,14] and nanowires directly grown on a current collector,[15] but the inherently high surface energy of Si in these forms is conducive to electrochemical sintering, resulting in the irreversible formation of dense agglomerates and deterioration of electrode performance.[16,17]

The stability of Si nanoparticles can be improved by encapsulation in a porous carbon matrix to form Si−C nanocomposites.[18−24] There are different methods of encapsulation with carbon. Ng et al.[20] reported improved performance by low temperature spray pyrolysis of a mixture of nanocrystalline Si powder (<100 nm) and citric acid in ethanol, but stability remained a problem. More recently, Hu et al.[22] reported a Si@SiO*x*/C nanocomposite in which preformed silicon nanoparticles were coated with carbon by hydrothermal carbonization of glucose. When combined with the use of vinylene carbonate additive in the electrolyte, stability up to 200 cycles at current densities of 150−1000 mA/g was obtained. Without the additive, however, the electrode was much less stable. Encapsulation can also be accomplished with varying degrees of improvement with carbonized resorcinol−formaldehyde (RF) gel.[18,23,24] Since preparation of a conductive, porous, carbon gel matrix is relatively simple, encapsulation in these matrices is an attractive method. Carbon gel matrices exhibit different properties depending on the preparation method, and properties such as pore size and rigidity could impact the ability of the matrix to accommodate the expansion/contraction of Si particles. It is also expected that the ability to maintain close contact of the carbon matrix with Si would be beneficial, and we hypothesized that this could be better achieved by covalent bonding between them. Thus, we prepared Si−C nanocomposites by carbonizing Si particles covalently bonded to RF gel by hydrosilylation.

Our samples were prepared starting from custom-preformed, H-terminated Si nanoparticles (HSi) (<30 nm, Meliorum Nanotechnology) that had some surface oxide. For samples Siy-PC-*n*, where *y* = wt % Si in the sample, *n* = sample number, and PC stands for phenolated composite. HSi was hydrosilylated with 2-allylphenol (**2AP**), which participated in RF polymerization, using a Pt catalyst to give HSi-2AP. Samples without hydrosilylation are labeled Siy-C-*n*. These particles, with or without surface functionalization, were dispersed in water and mixed with resorcinol, formaldehyde, and Na_2CO_3 in a sealed vial. The mixture was converted to a gel at 70 °C, aged, and then carbonized in an argon atmosphere at 700 °C (Scheme S1 and Table S1 in Supporting Information for preparation conditions).

* Corresponding author. E-mail: hkung@northwestern.edu.

(1) Winter, M.; Brodd Ralph, J. *Chem. Rev.* **2004**, *104*, 4245–4269.
(2) Whittingham, M. S. *MRS Bull.* **2008**, *33*, 411–419.
(3) Bruce, P. G.; Scrosati, B.; Tarascon, J.-M. *Angew. Chem., Int. Ed.* **2008**, *47*, 2930–2946.
(4) Cheng, F.; Tao, Z.; Liang, J.; Chen, J. *Chem. Mater.* **2008**, *20*, 667–681.
(5) Kasavajjula, U.; Wang, C. S.; Appleby, A. J. *J. Power Sources* **2007**, *163*, 1003–1039.
(6) Besenhard, J. O.; Yang, J.; Winter, M. *J. Power Sources* **1997**, *68*, 87–90.
(7) Huggins, R. A. *J. Power Sources* **1999**, *82*, 13–19.
(8) Larcher, D.; Beattie, S.; Morcrette, M.; Edstroem, K.; Jumas, J. C.; Tarascon, J. M. *J. Mater. Chem.* **2007**, *17*, 3759–3772.
(9) Boukamp, B. A.; Lesh, G. C.; Huggins, R. A. *J. Electrochem. Soc.* **1981**, *128*, 725–729.
(10) Beattie, S. D.; Larcher, D.; Morcrette, M.; Simon, B.; Tarascon, J. M. *J. Electrochem. Soc.* **2008**, *155*, A158–A163.
(11) Gao, B.; Sinha, S.; Fleming, L.; Zhou, O. *Adv. Mater.* **2001**, *13*, 816.
(12) Li, H.; Huang, X. J.; Chen, L. Q.; Wu, Z. G.; Liang, Y. *Electrochem. Solid State Lett.* **1999**, *2*, 547–549.
(13) Graetz, J.; Ahn, C. C.; Yazami, R.; Fultz, B. *Electrochem. Solid State Lett.* **2003**, *6*, A194–A197.
(14) Takamura, T.; Uehara, M.; Suzuki, J.; Sekine, K.; Tamura, K. *J. Power Sources* **2006**, *158*, 1401–1404.
(15) Chan, C. K.; Peng, H. L.; Liu, G.; McIlwrath, K.; Zhang, X. F.; Huggins, R. A.; Cui, Y. *Nat. Nanotechnol.* **2008**, *3*, 31–35.
(16) Li, H.; Huang, X. J.; Chen, L. Q.; Zhou, G. W.; Zhang, Z.; Yu, D. P.; Mo, Y. J.; Pei, N. *Solid State Ionics* **2000**, *135*, 181–191.
(17) Dimov, N.; Kugino, S.; Yoshio, M. *Electrochim. Acta* **2003**, *48*, 1579–1587.
(18) Wang, G. X.; Ahn, J. H.; Yao, J.; Bewlay, S.; Liu, H. K. *Electrochem. Commun.* **2004**, *6*, 689–692.
(19) Yang, X. L.; Wen, Z. Y.; Zhu, X. J.; Huang, S. H. *Electrochem. Solid State Lett.* **2005**, *8*, A481–A483.
(20) Ng, S. H.; Wang, J. Z.; Wexler, D.; Konstantinov, K.; Guo, Z. P.; Liu, H. K. *Angew. Chem., Int. Ed.* **2006**, *45*, 6896–6899.
(21) Wang, W.; Kumta, P. N. *J. Power Sources* **2007**, *172*, 650–658.
(22) Hu, Y. S.; Demir-Cakan, R.; Titirici, M. M.; Muller, J. O.; Schlogl, R.; Antonietti, M.; Maier, J. *Angew. Chem., Int. Ed.* **2008**, *47*, 1645–1649.
(23) Jung, Y. S.; Lee, K. T.; Oh, S. M. *Electrochim. Acta* **2007**, *52*, 7061–7067.
(24) Hasegawa, T.; Mukai, S. R.; Shirato, Y.; Tamon, H. *Carbon* **2004**, *42*, 2573–2579.

10.1021/cm8022314 CCC: $40.75
Published on Web 12/19/2008

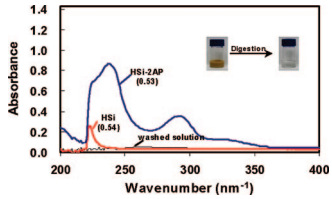

Figure 1. UV−vis spectra of digested HSi and HSi-2AP, showing absorption at 220 nm due to −Si−O− and phenolic absorption at 238 and 291 nm. Numbers in brackets are mg/mL.

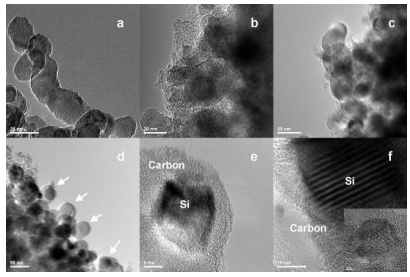

Figure 2. TEM images of (a) HSi; (b) Si27-PC; (c) Si45−C-3; (e) Si27-PC; and (f) Si45-PC-2. In part d, arrows highlight particles not encapsulated.

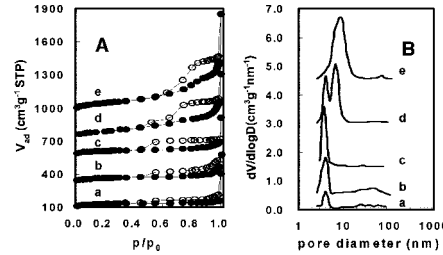

Figure 3. (A) N_2 adsorption/desorption isotherms at 77 K and (B) pore size distributions of (a) Si27-PC, (b) Si45-PC-1, (c) Si45-PC-2, (d) Si45-C-3, and (e) Si45-C-4. The isotherms and pore size distributions are displaced for clarity.

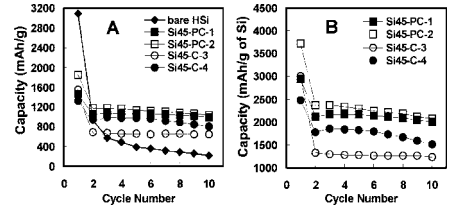

Figure 4. (A) Charge (lithiation) capacities based on total weight of Si and carbonized gel of HSi and nanocomposites and (B) charge capacities based on Si. Discharge rate ≈ 0.17 C.

Surface treatment of HSi by hydrosilylation can be followed with FTIR (Figure S1, Supporting Information). HSi showed distinct bands at 2250 and 2090 cm^{-1} for ν(H−Si)O_3 and ν(H−Si≡), respectively. After hydrosilylation, these bands were substantially reduced in intensity, while new bands for C−H stretching (2800−3000 cm^{-1}) and C−H bending (1500 cm^{-1}) appeared. From the decrease in total integral intensity of the H−Si bands, it was estimated that ∼54% of these groups were consumed by the reaction. The phenolic groups on these Si particles were quantified by UV−vis spectroscopy of samples digested in KOH solution (Figure 1). Using extinction coefficients (40 976 and 19 635 M^{-1} cm^{-1} at 238 and 291 nm, respectively) derived from a structurally similar model compound (Scheme S2, Figure S2, Supporting Information), the surface coverage of phenolic groups in HSi-2AP was estimated to be 0.16−0.2 mmol/g, which corresponds to 40−50% of surface H−Si groups on densely packed, 20 nm spherical Si nanoparticles.

XRD patterns (Figure S3, Supporting Information) of the carbonized samples showed only Si diffraction. The absence of graphite diffraction suggests an amorphous carbonized matrix with very small graphitic domains. The fact that the widths of the Si peaks were similar for different samples suggested little sintering due to carbonization. Using the Scherrer equation, the Si particles were estimated to be 20−22 nm in diameter, including the as-received sample.

TEM images confirmed encapsulation of the Si particles and their particle sizes to be ∼20 nm for HSi (Figure 2a) and nanocomposites (Figure 2b−d). For samples Si27-PC and the Si45-PC series, most of the Si particles were covered by carbon (images b, c, e, and f). However, particles not encapsulated by carbon were more readily detected in Si45-C-3 (image d) that was prepared by carbonizing a gel formed from a physical mixture of HSi and RF polymer precursors. The pore sizes and size distributions of these samples are shown in Figure 3. The hystereses in the isotherms over the pressure range ($p/p_0 = 0.4-1.0$) indicate the presence of mesopores. In addition, these samples also possess appreciable BET surface areas of 350−500 m^2/g due to microporosity. Table S2 (Supporting Information) summarizes the properties of the samples.

The charge (lithiation)/discharge (delithiation) behavior were measured in a Swagelok cell using Li as the counter electrode, 1.0 M $LiPF_6$ in 1/1 (v/v) ethylene carbonate−dimethylcarbonate as electrolyte, and porous polypropylene membrane as separator. The cells were galvanostatically cycled with cutoff voltages at 0.01 and 2.0 V. The samples were compared with respect to the magnitude of the reversible storage capacity, % irreversible loss of capacity in the first cycle, cycling stability of reversible capacity, and Coulombic efficiency.

Figure 4 shows the charge capacities of samples with cycle number. The capacity of bare Si nanoparticles without carbon encapsulation declined rapidly, losing over 60% of the capacity in the first cycle and over 90% after 10 cycles, consistent with literature results.[10,22,23] All encapsulated samples Si45-PC-1 and -2 and Si45-C-3 and -4 showed much improved stability, registering smaller initial drops and losses over 10 cycles. At the end of the 10th cycle, their capacities remained high, ranging from 640 to 1029 mA h/g. Because carbon constituted >50% of the composites and has much lower storage capacity than Si, the composites have lower theoretical capacities. By assuming a theoretical capacity of graphite for the carbonized RF gel (372 mA h/g) and subtracting its contribution from the measured data, the storage capacity assignable to Si can be estimated, which is shown in Figure 4B. Si45-PC-1 and Si45-PC-2, which were prepared with phenol functionalized SiNPs, retained over 56% of theoretical capacity of Si after 10 cycles, whereas Si45-C-3 and Si45-C-4 retained 35 and 42%, respectively. Retention of the reversible storage capacities were Si45-PC-1 (95%) > Si45-C-3 (93%) ≫ Si45-PC-2 (87%) > Si45−C-4 (86%). On the other hand, the irreversible capacity losses in the first cycle were: Si45-PC-1 (28%) ≈ Si45-C-4 (28%) <

Table 1. Dependence of Reversible Storage Capacity Degradation on Carbonization Temperature[a]

reference	*T*, °C	initial capacity, mA h/g	capacity drop and test conditions
18	650	1450	<5% drop after 50 cycles 145 mA/g, 0.02−2.0 V
this work	700	870−1180 (Si/R = 2.2)	3−14% drop after 10 cycles 100 mA/g, 0.01−20 or 0.02−1.5 V
23	1000	930 (Si/R = 1.8)	75% drop after 10 cycles 50 mA/g, 0−2 V
24	1000	980 (Si/R = 2)	35% drop after 3 cycles
	1100	1000 (Si/R = 2)	43% drop after 3 cycles
	1200	970 (Si/R = 2)	38% drop after 3 cycles all at 25mA/g, 0−1.5 V

[a] Si/R: molar ratio of Si and resorcinol in initial mixture.

Si45-PC-2 (36%) ≪ Si45-C-3 (56%). Finally, the Coulombic efficiencies varied as Si45-PC-1 and Si45-PC-2 (93−95%) > Si45-C-3 and Si45-C-4 (86−91%) (Figure S5, Supporting Information). We believe that higher capacities and Coulombic efficiencies of samples prepared with phenol-functionalized nanparticles are consequences of better contact between the carbon matrix and the Si particles.

There is no clear trend representing the effect of covalent bonding on cycling stability or initial irreversible loss. In addition to maintaining physical contact with the carbon matrix, cycling stability also depends on factors such as the tendency of Si particles to fracture or sinter and slow changes in the poorly understood solid electrolyte interface (SEI) layer. These are properties of regions of the electrode assembly away from the Si−carbon interface. In fact, in the case of particle fracture, one would expect the ductility of the carbon matrix to be an important factor. Indeed, data from this work and the literature (Table 1) points to a dependence of the cycling stability of carbon-encapsulated Si on the carbonization temperature of the RF gel: better stability for lower carbonization temperature. We hypothesize that this is a reflection of the different degrees of rigidity of the carbon matrices and their corresponding abilities to accommodate Si particle volume changes during cycling. It is known that the chemical composition of the RF gel changes during carbonization. The gel loses carbon, oxygen, and hydrogen upon heating, primarily as carbon oxides and water. In addition, hydrogen is also lost above ∼550 °C.[25] When the 700 °C-carbonized RF gel (without Si) prepared in this study was measured by TGA in N_2, a 7.7% weight loss was observed between 700 and 1000 °C, consistent with further dehydrogenation of the sample (Figure S6, Supporting Information). We believe that the carbon matrix becomes increasingly more rigid as hydrogen is lost, increasing the stress on the Si particle as the latter expands upon lithiation, causing it to fracture, and some fragments lose contact with the carbon matrix when the Si particle contracts upon delithiation, resulting in loss of storage capacity.

The irreversible capacity loss in the first cycle is commonly associated with the formation of the SEI layer due to reaction of Li^+ with the electrolyte and surface SiO. It is characterized by the reduction peak in the differential capacity curve at 0.3−1.0 V (vs Li/Li^+) that disappears after the first cycle (Figure S7, Supporting Information).[26,27] The integrated areas of this reduction peak were in the order: Si45-C-3 ≫ Si45-PC-2 > Si45-PC-1 ≈ Si45-C-4, paralleled the magnitude of the observed irreversible capacity losses.

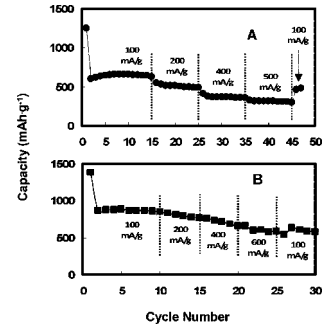

Figure 5. Charge (lithiation) capacities at different current densities for (A) Si27-PC, cycled at 0.01−2.0 V, charge and discharge currents were the same as indicated. (B) Si45-PC-1, cycled at 0.02−1.5 V with different discharge rates at a fixed charge rate of 100 mA/g.

The rate capabilities were measured for Si27-PC and Si45-PC-1 (Figure 5). For sample Si27-PC, the reversible charge capacity was around 630 mA h/g at C/6. It dropped slightly with increasing rates to a still respectable ∼300 mA h/g at about 1.7 C. Upon returning the discharge current to 100 mA/g after a total of 45 cycles, the reversible capacity dropped to 481 mA h/g (76% of fresh sample). For Si45-PC-1 and with a slightly different test condition, there were no obvious step decreases in capacity with increasing discharge current. It delivered about 590 mA h/g even at a high current of 600 mA/g (∼1 C). However, when the discharge current was returned to 100 mA/g after the 25th cycle, the capacity recovered to only 610 mA h/g (72% of the initial 850 mA h/g). The capacity loss is faster at higher current as others have observed. Nonetheless, even at high discharge rates, the samples prepared with phenolated particles showed high reversible capabilities with appreciable cycling stability, illustrating the beneficial effect of their preparation method.

In conclusion, we have shown clear benefits to forming covalent bond between a Si particle surface and the RF gel before carbonization. The Si-PC samples showed higher gravimetric capacity and Coulombic efficiency than the corresponding samples prepared from a physical mixture of bare HSis and RF polymer precursors. Even at high discharge rates, the Si-PC samples showed high reversible capacities. However, they still exhibit long-term cycling capacity loss, which needs to be improved further. The fact that the encapsulation process is experimentally rather simple, inexpensive, and easily scalable makes it an attractive method to improve electrochemical performance of nanostructured electrodes.

Acknowledgment. This work is supported by the Center for Energy Efficient Transportation at Northwestern University and US DOE, Basic Energy Sciences, Grant DE-FG02-01ER15184.

Supporting Information Available: Experimental details and supporting figures and tables (PDF). This material is available free of charge via Internet at http://pubs.acs.org.

CM8022314

(25) Wang, X.; Liang, C.; Dai, S. *Langmuir* **2008**, *24*, 7500–7505.
(26) Ota, H.; Sakata, Y.; Inoue, A.; Yamaguchi, S. *J. Electrochem. Soc.* **2004**, *151*, A1659–A1669.
(27) Pollak, E.; Salitra, G.; Baranchugov, V.; Aurbach, D. *J. Phys. Chem. C* **2007**, *111*, 11437–11444.